ACS Photonics

pubs.acs.org/journal/apchd5

Article

Continuous Lines of Topological Singularities in Metasurface Scattering Matrices: From Nodal to Exceptional

Jingguang Chen,[‖] Wenzhe Liu,*[,‖] Jiajun Wang, Changxing Li, Ruo-Yang Zhang, Xiaohan Cui, Fang Guan, Lei Shi, Jian Zi,* and C. T. Chan*

Cite This: https://doi.org/10.1021/acsphotonics.5c00575

Read Online

ACCESS | Metrics & More | Article Recommendations | Supporting Information

ABSTRACT: Topological properties of Hamiltonian matrices are well studied. However, photonic systems, often open, interact with their environment, and scattering matrices are used to characterize this interaction. Scattering matrices can exhibit their own unique topological features. We demonstrate that two-dimensional periodic photonic systems with open boundaries exhibit continuous lines of topological singularities (eigenvalue degeneracies) in their scattering matrices that are protected by mirror symmetry. In the three-dimensional frequency-momentum space, we find diabolic points and nodal lines, which transform into exceptional points and lines with material loss. These features in the scattering matrix's eigenvalue structure appear as vortex lines in the cross-polarization scattering phase, linking the eigen-problem to observable phenomena. We demonstrate these effects numerically and experimentally using a reflective nonlocal metasurface. Our findings extend the understanding of symmetry-protected continuous topological singularities to the realm of scattering matrices, opening new avenues for novel photonic devices and advanced wavefront engineering techniques.

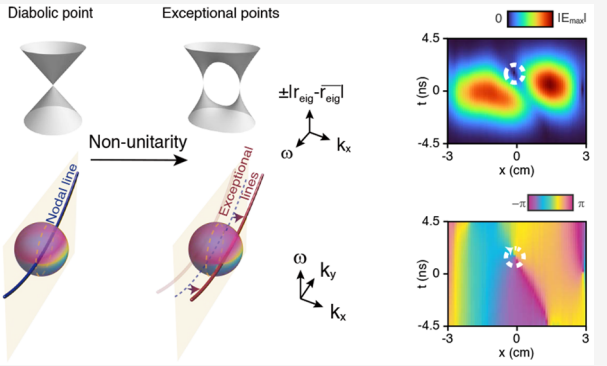

KEYWORDS: *topological singularity, scattering, nodal line, exceptional point, exceptional line, metasurface*

INTRODUCTION

Topological photonics has emerged as a vibrant field, leveraging concepts from topological insulators and other condensed matter systems. In these closed condensed matter systems, the properties of modes, such as band structures, are often described using Hamiltonian matrices, which can exhibit lines of topological singularities such as nodal lines (NLs) in a three-dimensional parameter space. Lifting these singularities leads to exotic transport effects like robust boundary states[1−9] and topological lasing.[10−13]

However, photonic systems are inherently open systems. To account for the coupling with the continuum in free space, one can apply an effective Hamiltonian approach derived from the Feshbach-Fano method, where the system's coupling to the continuum is treated as "radiative loss", manifested as an imaginary part of the Hamiltonian.[14−16] In the context of topological photonics, when this imaginary part is neglected, topological singularities such as NLs can still be observed. Including the imaginary part transforms the Hamiltonian into a non-Hermitian form, giving rise to exceptional lines (ELs) formed by exceptional points (EPs). EPs and ELs play crucial roles in fascinating physical phenomena like non-Hermitian skin effects,[17−21] and they enable novel optical functionalities such as enhanced sensing[22−26] and topological winding.[27−29]

While the Feshbach-Fano method provides important insights, it remains an approximation. A more precise description of open photonic systems is afforded by the scattering matrix formalism, which does not rely on such approximations. The scattering matrix can be compared to a time evolution operator, $\exp(-iH\chi)$, where H is a Hamiltonian and χ is the evolution parameter. This raises an intriguing question: can continuous lines of topological singularities like NLs or ELs appear in the scattering matrices of open photonic systems?

In this work, we discover and systematically characterize continuous lines of topological singularities in the scattering matrices of open periodic photonic systems such as nonlocal metasurfaces. We demonstrate that the unitary scattering matrix of a system with no material loss exhibits diabolic points (DPs) protected by mirror symmetry, which form continuous NLs in the frequency-momentum space. Herein, unitarity in a scattering matrix is analogous to Hermiticity in a Hamiltonian

Received: March 12, 2025
Revised: May 1, 2025
Accepted: May 1, 2025

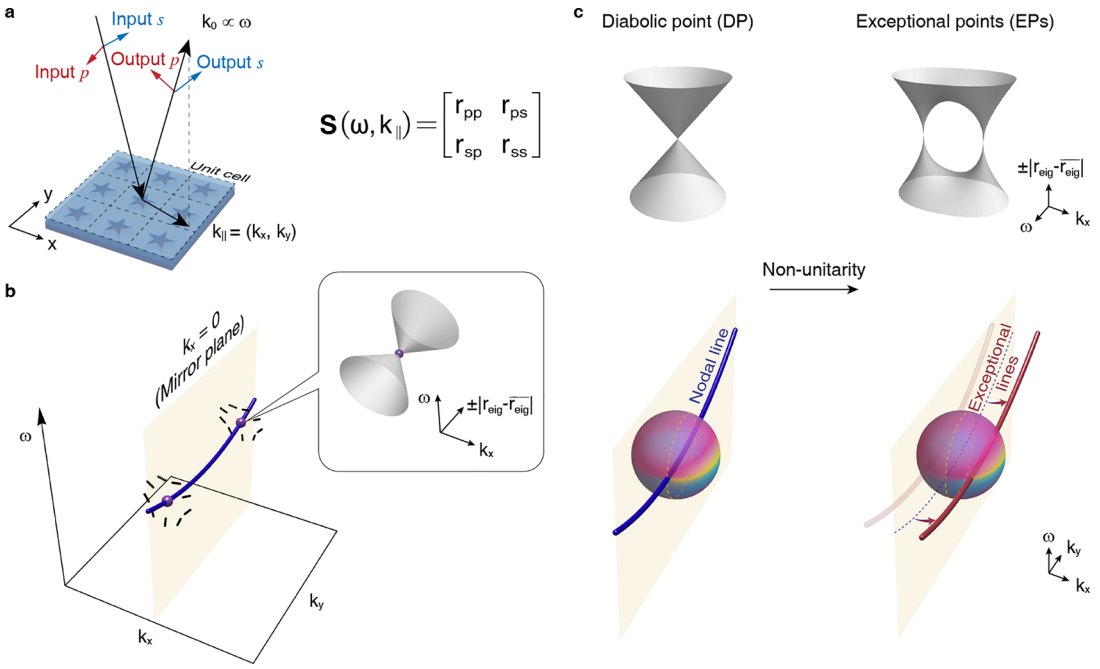

Figure 1. Degeneracies as topological singularities of scattering matrices. (A) Illustration of the system under investigation. A periodic structure on top of a mirror substrate is used to construct the basic 2 × 2 scattering matrix **S**. The scattering process is studied for in-plane momentum $\mathbf{k}_{\parallel}$ and frequency ω, without considering transmission and diffraction. This simplification confines the scattering channels to two reflecting plane waves with orthogonal polarizations. The polarization basis is naturally chosen to be *p* and *s* polarizations. (B) System's mirror symmetry about the $x = 0$ plane ensures the presence of nodal lines (NLs) in the $k_x = 0$ plane of the ω-$\mathbf{k}_{\parallel}$ parameter space. Each NL consists of diabolic points (DPs), which are characterized by the linear intersection of eigenvalues of the scattering matrix. (C) When material loss is considered, DPs evolve into exceptional points (EPs), resulting in the division of NLs into pairs of exceptional lines (ELs). This change is also reflected in the cross-polarization scattering phase in the ω-$\mathbf{k}_{\parallel}$ parameter space, where the phase vortices, originally located on the NL, are displaced due to the formation of ELs.

matrix. Incorporating material loss breaks unitarity, transforming these NLs into pairs of ELs. The resulting EPs have gained strong attention in flat optics and metamaterials.[27−33] Remarkably, these continuous lines of singularities give rise to topological darkness[34−38] and phase vortex lines in the cross-polarization scattering phase maps. We experimentally demonstrate the generation of spatiotemporal vortices based on these singularities. Our findings extend the concepts of topological photonics to continuous lines of singularities in scattering matrices, revealing new avenues for exploration and application.

RESULTS AND DISCUSSION

Basic Principles. To establish the theoretical foundation and reveal the existence of topological singularities in scattering matrices, we construct an optical system with the simplest 2 × 2 scattering matrix − a reflection-only periodic structure, schematically illustrated in Figure 1a. The plane-wave scattering process of such a structure is characterized by a specific in-plane wavevector $\mathbf{k}_{\parallel}$, and there are two orthogonally polarized scattering channels. Choosing a *p*-*s* basis of polarization, the scattering matrix **S** of the system is expressed as

$$\mathbf{S}(\omega, \mathbf{k}_{\parallel}) = \begin{bmatrix} r_{pp}(\omega, \mathbf{k}_{\parallel}) & r_{ps}(\omega, \mathbf{k}_{\parallel}) \\ r_{sp}(\omega, \mathbf{k}_{\parallel}) & r_{ss}(\omega, \mathbf{k}_{\parallel}) \end{bmatrix} \tag{1}$$

Here, ω is the real angular frequency of the scattering process, which determines the free-space wavevector $\mathbf{k}_0$. The subscripts of reflection coefficients r_{ij} represent the polarization channels *p* and *s*. The *s* channel is perpendicular to the incident plane and parallel to the sample plane, while the *p* channel is in the incident plane and perpendicular to the input and output free-space wavevectors.

The nondiagonal entries of the scattering matrices (r_{sp} and r_{ps}) are generally nonzero for a $\mathbf{k}_{\parallel}$ without any symmetry, which induces interchannel scattering. Consequently, the eigenvalues of the scattering matrices cannot form a linear crossing and there will be a "gap" between them.

However, symmetry may make things different. Assuming that our system has mirror symmetry about $x = 0$, if $\mathbf{k}_{\parallel}$ is in the corresponding momentum-space mirror plane $k_x = 0$, the scattering matrix must be invariant under a reflection operation:

$$\begin{aligned} &\mathbf{S}(\omega, \mathbf{k}_{\parallel}) = \mathbf{M}\mathbf{S}(\omega, \mathbf{k}_{\parallel})\mathbf{M}^{-1}, \\ &\mathbf{M} = \begin{bmatrix} 1 & 0 \\ 0 & -1 \end{bmatrix} (\text{even}), \\ &\text{or } \mathbf{M} = \begin{bmatrix} -1 & 0 \\ 0 & 1 \end{bmatrix} (\text{odd}) \\ &\Leftrightarrow r_{ps} = r_{sp} = 0 \end{aligned} \tag{2}$$

Here, "even" and "odd" refer to the eigenvalues of the reflection symmetry operator with respect to the $x = 0$ plane. An "even" symmetry corresponds to an eigenvalue of +1, maintaining the input/output vector's direction, while an "odd" symmetry results in an eigenvalue of −1, reversing its direction. This mirror symmetry enforces zero interchannel coupling between the even-mirror-parity and odd-mirror-parity channels, resulting in a diagonal scattering matrix ($r_{ps} = r_{sp} =$

https://doi.org/10.1021/acsphotonics.5c00575
ACS Photonics XXXX, XXX, XXX−XXX

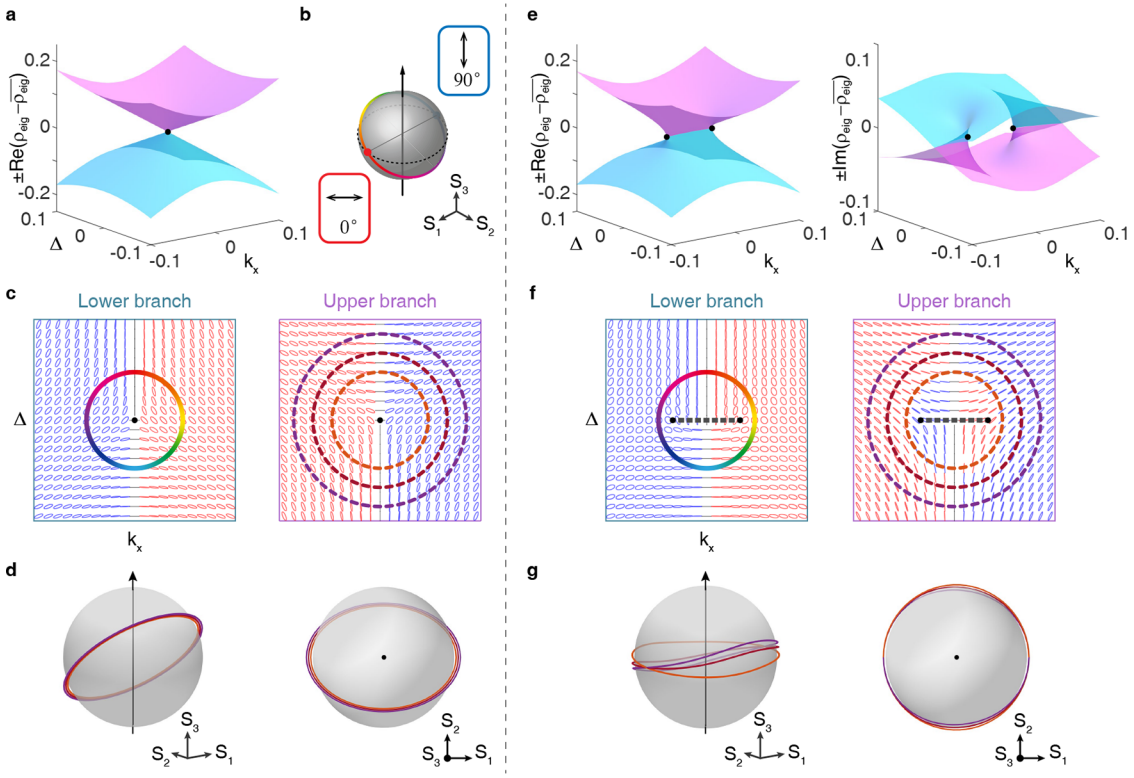

Figure 2. Demonstration of scattering-matrix topological singularities in lossless and lossy theoretical systems using small momentum (k_x) and frequency ($\Delta = \omega - \omega_0$) expansion. (A) Two eigenvalue surfaces of the scattering matrix's "core" with the mean value subtracted, exhibiting a DP where the two eigenvalue branches intersect linearly in a lossless system. Note that the core's eigenvalues have no imaginary part, unlike those of a true scattering matrix. (B) Mirror symmetry causes a loop in the ω-k_x space surrounding the DP to trace a great circle on the Poincaré sphere. The mirror symmetry-enforced vertical and horizontal polarizations in the ω-k_x space map to antipodal points on the Poincaré sphere's equator. The mirror-symmetric polarization distribution results in an inversion symmetric trajectory on the Poincaré sphere that enables robust cross-polarization scattering phase vortex, provided the input/output polarization lies outside the loop. (C) Eigen-polarization maps for the lower and upper branches in the lossless case, with colored circles in the upper-band map indicating different momentum-space trajectories around the DP. (D) Side and top views of the Poincaré sphere showing the projections of the three trajectories from (C), demonstrating mirror-symmetry-protected winding on the sphere. (E) Material loss splits the DP into two EPs, showing both real and imaginary parts of the eigenvalues. (F) Modified eigen-polarization maps in the lossy case, where dashed lines indicate the branch cuts between EPs. (G) Corresponding Poincaré sphere projections showing how the three trajectories are modified by the presence of EPs, with side and top views revealing the preserved topological structure.

0). Consequently, the polarization channels p and s become the eigen-polarization channels, with r_{pp} and r_{ss} representing the eigenvalues of the scattering matrix.

If we further assume that there is no material loss, the scattering matrix must be unitary, meaning $|r_{pp}| = |r_{ss}| = 1$. Therefore, they can be expressed as exponentials of two unimodular real numbers: $r_{pp} = e^{i\phi_p}$ and $r_{ss} = e^{i\phi_s}$. For each k_y with $k_x = 0$, we can tune ω to make ϕ_p (r_{pp}) cross ϕ_s (r_{ss}) linearly, leading to the existence of a diabolic point (DP) for both the phases and the eigenvalues in the $\omega - \mathbf{k}_{\parallel}$ space. If we move away from the mirror plane, the crossing is lifted. It results in conical eigenvalue surfaces. Due to the unitarity of the matrix, the two eigenvectors of the scattering matrix remain orthogonal to each other. This is the topological degeneracy we are looking for. While DPs in scattering matrices have been largely overlooked, they play a fundamental role in understanding topological singularities in open systems.

Note that, $\phi_p = \phi_s$ can be satisfied on continuous curves in the $k_x = 0$ plane since we have two real number degrees of freedom, ω and k_y. This implies that there will be DPs forming NLs in the mirror plane, as illustrated in Figure 1b. We expect topological behavior around a NL similar to that in Hamiltonian matrices − the eigenvectors of the scattering matrix will form polarization vortex lines around the NL,[8,9,39−43] and such vortex lines in the eigenvectors will lead to vortex lines of cross-polarization scattering phase [Pancharatnam-Berry (PB) phase] that are robustly pinned in the mirror-symmetric k plane on the NL, as shown in the left panel of Figure 1c. Importantly, these phase vortices are directly observable through spectroscopic measurements of the scattering matrix elements, in contrast to the phase winding in Hamiltonian systems which typically requires adiabatic evolution of states to be observed. This direct accessibility of topological features makes our scattering matrix approach particularly advantageous for experimental investigations.

Material loss is difficult to avoid in practical structures. When material loss is considered, energy is no longer conserved during the scattering process, breaking the unitarity of the scattering matrix. Consequently, the orthogonality between the eigenvectors of the scattering matrix is lost, allowing the existence of exceptional points (EPs) where both eigenvalues and eigenvectors coalesce.[44] EPs in scattering matrices have been studied in various contexts, from coherent perfect absorption[45,46] to "chiral" exceptional points, and their applications in flat optics have been demonstrated by M. Lawrence et al.,[27−32] but the connection between scattering matrix NLs and continuous lines of EPs has not been fully uncovered. In fact, EPs will emerge from DPs, such as those in

https://doi.org/10.1021/acsphotonics.5c00575
ACS Photonics XXXX, XXX, XXX−XXX

the lossless case discussed above, as illustrated in Figure 1c. This is analogous to EPs in eigen-energy levels emerging from DPs in Hamiltonian matrices.[47−50] Here, the NL will evolve into a pair of ELs that are mirror-symmetric about $k_x = 0$. Correspondingly, the robustness of the PB-phase vortex induced by the topological singularity is reduced. The phase vortex will shift away from the position of the original DP, and it will move around under different cross-polarization input-output setups. However, it will not vanish due to its topological nature. If we consider an input that is the same as the eigenvector of one of the EPs and the output to be orthogonal to the eigenvector, the phase vortex will coincide with the EP.

Theoretical Demonstration. To substantiate the above predictions and the existence of topological singularities, we apply a temporal coupled mode theory (TCMT) model. We assume the system has only two resonances in the frequency range of interest, and their eigenfrequencies are $\omega_1(\mathbf{k}_\parallel)$ and $\omega_2(\mathbf{k}_\parallel)$, whose subscripts mark the corresponding resonances. These resonances form photonic bands, and they can be of either even or odd mirror parity about the mirror plane $k_x = 0$. Thus, there can be three combinations of mirror parities, "even + even", "odd + odd" and "even + odd" (equivalent to "odd + even"). Neglecting the material loss, we have the radiative-loss-induced decay ratios, expressed by $\gamma_{11}(\mathbf{k}_\parallel)$ and $\gamma_{22}(\mathbf{k}_\parallel)$, of the resonances. Note that the resonances can also couple by radiation, inducing radiation coupling ratios $\gamma_{21}(\mathbf{k}_\parallel)$ and $\gamma_{12}(\mathbf{k}_\parallel)$. For simplicity, we only consider resonances with $\mathbf{k}_\parallel = (k_x, 0)$, and we denote $\omega_1(0)$, $\omega_2(0)$, $\gamma_{11}(0)$, $\gamma_{22}(0)$ by ω_1, ω_2, γ_{11}, γ_{22}. It is important to note that the minimum number of resonances required to demonstrate the topological singularity is two, although more resonances can be included to explore more complex scenarios which appear in practical photonic systems. This number of resonances is independent of the dimension of the scattering matrix, which is 2×2 due to the two polarizations of light. After some derivations [see Supporting Information], we obtain the expressions of the scattering matrix with small ω-$\mathbf{k}_\parallel$ expansions performed:

$$\mathbf{S}(\omega = \omega_0 + \Delta, k_x) \approx r\left\{\mathbf{I} - \frac{1}{2}\xi\left[\underline{\Delta(C_1\mathbf{I} \mp C_1\sigma_z) + k_x(C_2\sigma_x \mp C_3\sigma_y)}\right]\right\} \quad (-\text{ for "even + even" and } + \text{ for "odd + odd"}) \tag{3}$$

or

$$\approx r\left\{\mathbf{I} - \frac{1}{2}\xi\left[(B - iA)\mathbf{I} + \underline{\Delta(C_0\mathbf{I} - C_1\sigma_z) + k_x(C_2\sigma_x - C_3\sigma_y)}\right]\right\} \quad (\text{for "even + odd"}) \tag{4}$$

Here, ω_0 is the central frequency around which we perform expansion, and it is determined by the properties of the two resonances at $k_x = 0$: $\omega_0 = (\omega_1\gamma_{22} + \omega_2\gamma_{11})/(\gamma_{22} + \gamma_{11})$ for the "even + even" and "odd + odd" parity combinations, or $\omega_0 = (\omega_1\gamma_{22} - \omega_2\gamma_{11})/(\gamma_{22} - \gamma_{11})$ for the "even + odd" case. r is the direct reflection coefficient under normal incidence, while ξ is a frequency-dependent factor that is not expanded since it does not affect the matrix's eigen-solutions. A, B and C_i ($i = 0, 1, 2, 3$) are real numbers, among which C_i is a number related to the i-th Stokes parameter of the resonances' eigen-radiation. $\sigma_{x,y,z}$ are the Pauli matrices.

One would observe that the "core" of the scattering matrix determining the eigen-solutions (the underlined parts) only has real and linear dependence on two degrees of freedom, the frequency Δ and wavevector k_x, for all the combinations. Consequently, the eigenvalues have linear dependence on Δ and k_x and will intersect at $\Delta = k_x = 0$, i.e., a DP is formed. As an example, we choose the "odd + odd" parity combination with $C_{0,1,2,3} = 1$ and plot the eigenvalues of the core, as visualized in Figure 2a. Note that the mean value of the eigenvalues has been subtracted for better visualization. A DP is clearly exhibited. We also plot the eigenvector polarization maps for the two eigenvalue branches as polarization ellipses in Figure 2c. The ellipses show topological winding behavior around the DP in the frequency-momentum space. If we project loops around the singularity in the Δ-k_x space onto the Poincaré sphere, we will find two antipodal points on the loops fixed on the equator, which are the vertical and horizontal polarizations enforced by the mirror symmetry as illustrated in Figure 2b. The trajectories connecting the two fixed points will be inversion-symmetric, tracing great circles, as a result of the mirror-symmetric polarization distribution. Our analysis can be verified by plotting three momentum-space trajectories at different distances from the DP (colored circles in the upper-band polarization map of Figure 2c) and their corresponding projections onto the Poincaré sphere in Figure 2d. Both side and top views of the sphere clearly show that all trajectories follow great circles and maintain the mirror-symmetry-enforced fixed points on the equator, confirming our theoretical prediction in Figure 2b. These trajectories give rise to a robust cross-polarization scattering phase vortex pinned at the DP, provided the input/output polarization states are chosen outside this great circle of eigenvector states. Such a choice ensures a continuous phase winding rather than a sudden jump.

Based on the above lossless system, we can further take material loss into consideration by adding perturbative nonradiative decay ratios to the two resonances, γ_{nr1} and γ_{nr2} respectively. This will introduce extra terms to the "core" of the scattering matrix,

$$\delta\mathbf{S}_{core} \approx i[(C_4\mathbf{I} \mp C_5\sigma_z) + k_x(C_6\sigma_x \mp C_7\sigma_y)] \quad (-\text{ for "even + even" and } + \text{ for "odd + odd"}) \tag{5}$$

As for the "even + odd" case, the expression shares the same form as that of the "even + even" case with a different definition of C_i. $C_{4,5,6,7}$ here are real numbers similar to $C_{0,1,2,3}$, but these numbers are proportional to γ_{nr}. It is obvious that the material loss introduces imaginary parts to the coefficients of the Pauli matrices, hence leading to the emergence of EPs from the original DPs. We assume $C_{4,5,6,7} = 0.05$ and plot both the real and imaginary parts of the eigenvalue surfaces in Figure 2e, where two EPs can be clearly identified. The corresponding eigenvector polarization maps in Figure 2f reveal a branch cut (dashed lines) connecting the two EPs, across which the eigenvector ellipses exhibit abrupt changes. The modification of topological structure by EP pairs can be examined by plotting the same three momentum-space trajectories as in the lossless case and their projections onto the Poincaré sphere in Figure 2g. The side and top views show that the mirror-symmetry-protected winding behavior persists.

https://doi.org/10.1021/acsphotonics.5c00575
ACS Photonics XXXX, XXX, XXX−XXX

Experimental Verification of the Singularities. To validate our theoretical predictions, we designed a nonlocal metasurface structure that operates in the microwave range, enabling the observation of topological singularities in scattering matrices. The nonlocal nature of the metasurface is essential here, as our investigation of singularities in the frequency-momentum parameter space requires the metasurface to exhibit momentum-dependent responses through collective interactions beyond individual meta-atoms, manifesting as angular dispersion in the system. This collective behavior is implemented through an array of split-ring resonators fabricated on a printed circuit board (PCB) with a mirror substrate, as schematically illustrated in Figure 3a. The

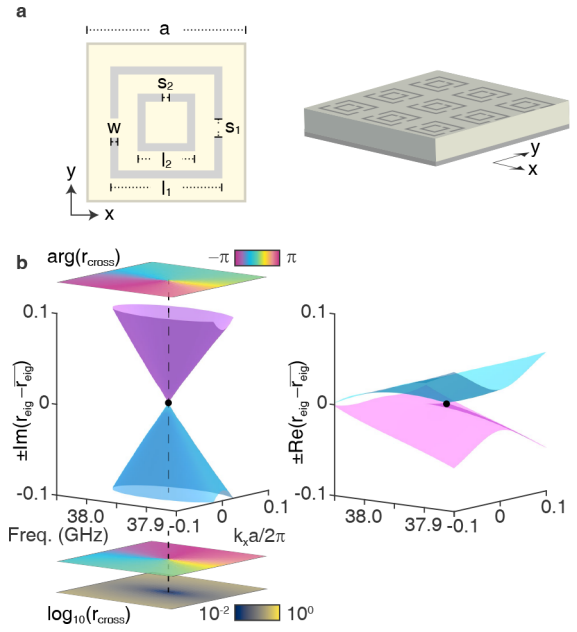

Figure 3. Nonlocal metasurface design for observation of topological singularities in scattering matrices. (A) Schematic of the designed nonlocal metasurface. The unit cell comprises two split-ring resonators fabricated on a printed circuit board (PCB) atop a mirror substrate. The geometric parameters are period a = 3.810 mm, outer ring side length l_1 = 2.670 mm, inner ring side length l_2 = 1.370 mm, line width w = 0.190 mm, outer ring split width s_1 = 0.460 mm, inner ring split width s_2 = 0.190 mm, and PCB thickness t = 0.381 mm. (B) Simulated eigenvalues of the scattering matrix for the designed metasurface, neglecting the loss of the PCB. The real and imaginary parts of the eigenvalues, with the mean value subtracted, are depicted. The analysis focuses on a representative DP near 38 GHz, chosen for clarity among numerous DPs present in the scattering matrix. The map above the eigenvalue surfaces shows the cross-polarization phase for 45° to −45° linear polarization conversion. The two maps below display the −45° to 45° cross-polarization phase (top) and the amplitude of the cross-polarized reflection coefficient (bottom).

unit cell of the metasurface includes two split-ring resonators with specific geometric parameters: period a = 3.810 mm, outer ring side length l_1 = 2.670 mm, inner ring side length l_2 = 1.370 mm, line width w = 0.190 mm, outer ring split width s_1 = 0.460 mm, inner ring split width s_2 = 0.190 mm. Additionally, the outer ring splits are offset by 0.133 mm toward the $-y$ direction. The PCB thickness is t = 0.381 mm. In the absence of material loss (dielectric constant ε_r = 4.3), the eigenvalues (with their mean value subtracted) of the metasurface's scattering matrix is obtained by simulations, and we focus our attention on a representative DP near 38 GHz for clarity (Figure 3b). The phase maps above and below the eigenvalue surfaces illustrate the cross-polarization phase for 45° to −45° and −45° to 45° linear polarization conversion, respectively. A phase singularity pinned at the DP's frequency and momentum can be observed in either map, corresponding to the zero point in the amplitude map of cross-polarized reflection coefficient. These ±45° cross-polarization configurations provide the most distinct visualization of the phase vortices associated with the DPs. These results confirm the presence of DPs and their associated phase vortices as predicted by our theoretical model. The DPs form an NL in the three-dimensional ω-$\mathbf{k}_\parallel$ parameter space [see Supporting Information].

When we include the effects of material loss in the PCB (dielectric constant $\varepsilon_r = 4.3 + 0.02i$), the simulations show a transformation in the scattering matrix's eigenvalues. Specifically, two EPs emerge by splitting from the original DP locations, accompanied by self-intersecting Riemann surfaces (Figure 4a). This shift in the eigenvalues' imaginary and real parts demonstrates the EPs' formation due to loss. The phase vortices in the phase maps move away from k_x = 0, reflecting the new positions of the EPs. Correspondingly, the eigenvectors of EPs are ± 45°polarization. Moreover, leveraging symmetry-breaking enable coalesced eigenvectors to access other polarization states.[51] For example, if inner ring split of unit cell is offset by a distance, i.e., the mirror symmetry is broken, the eigenvectors of EPs are general elliptical polarization [see Supporting Information]. Figure 4b presents slices of the −45° to 45° cross-polarization phase maps along with the corresponding eigenvalue structures at different values of k_y. These slices reveal that while tilting the incident plane (varying k_y) shifts the positions of the singularities in the ω-k_x plane, the fundamental structure of paired EPs remains intact, protected by the underlying mirror symmetry. The continuous existence of these singularities across different k_y values forms a vortex line in the ω-$\mathbf{k}_\parallel$ parameter space, corresponding to an EL [see Supporting Information for the ELs directly mapped in the three-dimensional ω-$\mathbf{k}_\parallel$ parameter space along with eigenvector maps sliced at different k_y, including results for both the with mirror symmetry and when mirror symmetry is broken]. This robustness of the singular line against tilting of the incident plane provides strong evidence for the symmetry-protected nature of these topological features, validating our theoretical predictions. We want to clarify that, while radiation loss in the Feshbach-Fano method introduces non-Hermiticity resulting in EPs and ELs within the Hamiltonian framework, this type of loss is not considered true loss in the scattering matrix approach. The scattering matrix formalism considers the photonic system and its environment on equal footing, including the continuum, meaning that radiation loss does not break unitarity that is analogous to Hermiticity. In contrast, nonunitarity arising from material loss affects the energy conservation within the system itself, which is comparable to non-Hermiticity in Hamiltonian. Therefore, only true material loss, leads to the formation of EPs and ELs in the scattering matrix formalism.

To further substantiate our findings, we conducted an experimental demonstration of spatiotemporal vortex generation enabled by the singularities in the ω-$\mathbf{k}_\parallel$ space. A Gaussian beam of −45° linear polarization, centered at around 38 GHz with a 0.15 GHz bandwidth and approximately 10° divergence angle, was directed onto the fabricated metasurface. The cross-polarization real-space frequency-domain response of the

https://doi.org/10.1021/acsphotonics.5c00575
ACS Photonics XXXX, XXX, XXX−XXX

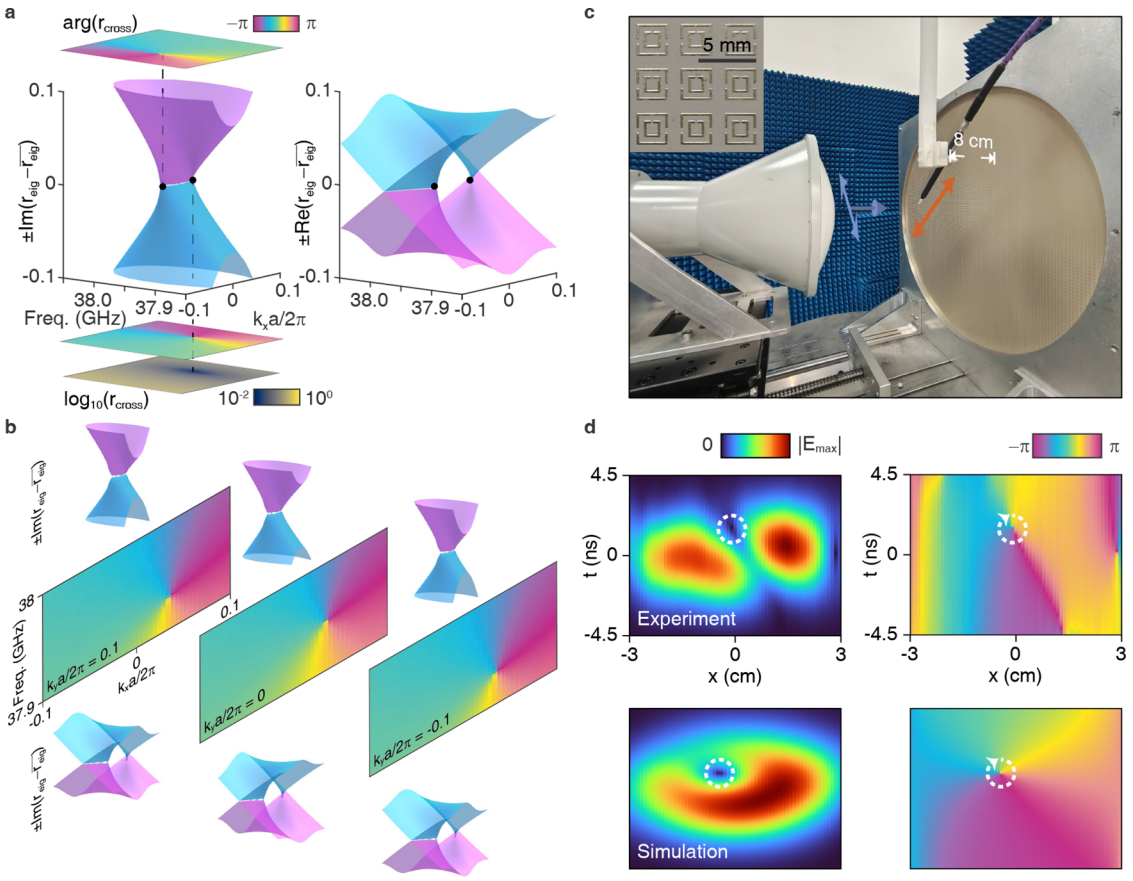

Figure 4. Observation of topological singularities via spatiotemporal vortex generation. (A) Simulated eigenvalues of the scattering matrix for the designed metasurface, accounting for the loss in the PCB. The real and imaginary parts of the eigenvalues (with the mean value subtracted) reveal two exceptional points (EPs) and self-intersecting Riemann surfaces. The phase vortices in the phase maps shift away from $k_x = 0$ with the emergence of EPs, no longer coinciding with each other. (B) −45° to 45° cross-polarization phase maps sliced at different values of k_y, marking the existence of a vortex line, corresponding to an EL, in the ω-$\mathbf{k}_\parallel$ parameter space. Insets above and below the phase maps show imaginary and real parts of the eigenvalues for each k_y, respectively. (C) Due to the presence of the EL in the frequency-momentum space, a spatiotemporal optical vortex can be generated and observed experimentally. A Gaussian beam with −45° linear polarization is impinged onto the fabricated metasurface, and the real-space frequency-domain response of the reflective sample is measured under 45° linear polarization. After performing a frequency-domain Fourier transform, the spatiotemporal profile of the reflected pulse is obtained. (D) Measured (upper panel) and simulated (lower panel) spatiotemporal profiles of the reflected pulse. The space-time intensity maps reveal zero points, while the phase maps exhibit phase vortices. Both profiles show similar pulse shapes and phase structures, validating the existence of the singularity line. The measured profile displays an additional dark line through the vortex center, likely arising from probe interference with the input and output pulses.

reflective sample was measured on a horizontal line 8 cm above the metasurface by a −45°-polarized magnetic field probe (i.e., a 45°-polarized electric field probe) [see Figure 4c for the experimental setup]. By performing a frequency-domain Fourier transform upon the measured field, we obtained the profile of the reflected cross-polarized pulse. We simulated the reflected pulse by applying the calculated cross-polarized reflection coefficient to an incident Gaussian pulse with the same parameters. The measured and simulated spatiotemporal profiles are compared in Figure 4d, both revealing zero points in intensity and phase vortices. While the measured profile shows an additional dark line through the vortex center, likely due to probe interference effects, the overall agreement between simulation and experiment provides strong evidence for the continuous line of singularities in the ω-$\mathbf{k}_\parallel$ space. These results confirm our theoretical predictions and add to the growing applications of scattering matrix singularities in photonics.[30−33]

DISCUSSION AND CONCLUSIONS

In this work, we have explored continuous lines of topological singularities in the scattering matrices of open periodic photonic systems. We theoretically predicted and demonstrated that mirror symmetry leads to the formation of diabolic points (DPs) and nodal lines (NLs) in the frequency-momentum space. We uncovered how material loss transforms these NLs into exceptional lines (ELs), revealing a fundamental connection between these distinct types of line singularities in scattering matrices. Our theoretical predictions were validated through the design, fabrication, and experimental characterization of a nonlocal metasurface structure operating in the microwave range.

Recent works[30−33,43] have demonstrated growing interest in understanding topological features of scattering matrices. For instance, through singular value decomposition (SVD) analysis, Guo et al. revealed previously undiscovered topological features of well-known scattering matrix singularities such as poles and zeros, which correspond to lasing states and coherent perfect absorption, respectively.[43] This surge of

https://doi.org/10.1021/acsphotonics.5c00575
ACS Photonics XXXX, XXX, XXX−XXX

research highlights the increasing need for a systematic understanding of scattering matrix degeneracies, particularly continuous lines of singularities.

Our study addresses this need by revealing the role of mirror symmetry in protecting continuous lines of singularities. While previous SVD-based approaches focus on singular values, our work explores different topological features through eigenvalue analysis, revealing both NLs and how material loss induce ELs that emerge from the coalescence of eigenstates. The scattering matrix framework we develop offers unique advantages for practical applications, particularly in sensitivity enhancement. Unlike Hamiltonian-based approaches[22−26] that may suffer from ensemble averaging effects in open systems, scattering matrices directly connect to measurable quantities and maintain their sensitivity even in lossy environments. This makes our findings particularly relevant for developing robust photonic devices for signal processing, communication, and sensing.

There are several exciting avenues for future research. One direction is to investigate different symmetries or higher-order topological effects in more complex systems with additional scattering channels. Additionally, exploring non-Abelian topological singularities or studying systems with more complex scattering matrices could reveal new physical phenomena. The principles demonstrated here could also be extended to other physical systems where scattering matrices play a crucial role, such as acoustics and electronics. By further exploring the interplay between topology and scattering in open systems, we can uncover new functionalities and design principles for next-generation photonic devices, contributing to a broader understanding of topological phenomena in physics.

MATERIALS AND METHODS

Experimental Verification of the Singularities. Here, we detail the experimental setup for measuring the spatiotemporal profile of the pulse. As illustrated in Figure S1a, the profile measurement system consists of a lens antenna and a polarized probe, both connected to a vector network analyzer (VNA, Keysight N5245B) via coaxial cables. The lens antenna functions as the source, emitting a Gaussian beam with −45° linear polarization toward the metasurface sample. The printed-circuit-board sample, comprising 110 × 110 unit cells of double split ring resonators Figure S1b, is mounted vertically on a sample rack. We define the y direction as the direction to which the gap of the inner ring points, with the sample oriented such that the y direction is upward. The +45° cross-polarized component of the reflected field is then detected by the probe, positioned along a horizontal straight line 8 cm above the sample.

To characterize the metasurface's response, we perform a frequency sweep of the Gaussian beam, obtaining the frequency-domain field reflected by the sample. We then apply a Gaussian filter in the frequency domain, which corresponds to a Gaussian pulse in the time domain. Subsequently, we conduct a Fourier transform on the filtered field to obtain the pulse profile. The resulting spatiotemporal profile of the pulse is presented and analyzed in the main text.

Simulations. To obtain the scattering matrices of the designed structure, we employed the finite element method (FEM). We modeled a single unit cell of the metasurface, incorporating an air pillar above it to account for the free space interaction. Bloch periodic boundary conditions were applied to the x- and y-direction boundaries of the unit cell to simulate an infinite array. In the z direction, we applied perfectly matched layers (PMLs) at the upper boundary to absorb outgoing waves without reflection, while the bottom boundary was set as a perfect electric conductor (PEC) to simulate the mirror substrate.

A domain-backed periodic port was positioned above the metasurface to generate the incident plane wave. A second port was used to capture the reflected field, allowing us to calculate the full scattering parameters of the structure. This simulation setup enabled us to accurately characterize the electromagnetic response of the metasurface and analyze the eigenvalues/eigenvectors of the scattering matrices.

ASSOCIATED CONTENT

Data Availability Statement

The data that support the findings of this study are available from the corresponding authors upon reasonable request.

Supporting Information

The Supporting Information is available free of charge at https://pubs.acs.org/doi/10.1021/acsphotonics.5c00575.

Temporal coupled mode theory (TCMT) model demonstrating the existence of topological singularities; 3D mapping of nodal line and exceptional lines of the designed nonlocal metasurface; experimental setup, pulse profile measuring system, and measured printed-circuit-board (PCB) sample; 3D mapping of the nodal line in the lossless non-local metasurface; 3D mapping of exceptional lines in the lossy non-local metasurface; and 3D mapping of exceptional lines in a lossy non-local metasurface with broken mirror symmetry (PDF)

AUTHOR INFORMATION

Corresponding Authors

Wenzhe Liu − *Institute for Nanoelectronic Devices and Quantum Computing and State Key Laboratory of Surface Physics, Key Laboratory of Micro- and Nano-Photonic Structures (Ministry of Education), and Department of Physics, Fudan University, Shanghai 200433, China; Department of Physics and Institute for Advanced Study, The Hong Kong University of Science and Technology, Hong Kong 999077, China;* orcid.org/0000-0002-6582-4161; Email: wzliu@fudan.edu.cn

Jian Zi − *Institute for Nanoelectronic Devices and Quantum Computing and State Key Laboratory of Surface Physics, Key Laboratory of Micro- and Nano-Photonic Structures (Ministry of Education), and Department of Physics, Fudan University, Shanghai 200433, China*; Email: jzi@fudan.edu.cn

C. T. Chan − *Department of Physics and Institute for Advanced Study, The Hong Kong University of Science and Technology, Hong Kong 999077, China;* orcid.org/0000-0002-9335-8110; Email: phchan@ust.hk

Authors

Jingguang Chen − *Institute for Nanoelectronic Devices and Quantum Computing and State Key Laboratory of Surface Physics, Key Laboratory of Micro- and Nano-Photonic Structures (Ministry of Education), and Department of Physics, Fudan University, Shanghai 200433, China*

Jiajun Wang − *State Key Laboratory of Surface Physics, Key Laboratory of Micro- and Nano-Photonic Structures*

https://doi.org/10.1021/acsphotonics.5c00575
ACS Photonics XXXX, XXX, XXX−XXX

(Ministry of Education), and Department of Physics, Fudan University, Shanghai 200433, China

Changxing Li − *State Key Laboratory of Surface Physics, Key Laboratory of Micro- and Nano-Photonic Structures (Ministry of Education), and Department of Physics, Fudan University, Shanghai 200433, China*

Ruo-Yang Zhang − *Department of Physics and Institute for Advanced Study, The Hong Kong University of Science and Technology, Hong Kong 999077, China;* orcid.org/0000-0002-3567-0499

Xiaohan Cui − *Department of Physics and Institute for Advanced Study, The Hong Kong University of Science and Technology, Hong Kong 999077, China*

Fang Guan − *Institute for Nanoelectronic Devices and Quantum Computing and State Key Laboratory of Surface Physics, Key Laboratory of Micro- and Nano-Photonic Structures (Ministry of Education), and Department of Physics, Fudan University, Shanghai 200433, China*

Lei Shi − *Institute for Nanoelectronic Devices and Quantum Computing and State Key Laboratory of Surface Physics, Key Laboratory of Micro- and Nano-Photonic Structures (Ministry of Education), and Department of Physics, Fudan University, Shanghai 200433, China*

Complete contact information is available at: https://pubs.acs.org/10.1021/acsphotonics.5c00575

Author Contributions

[‖]J.C. and W.L. contributed equally to this work.

Funding

This work was supported by the National Natural Science Foundation of China (No. 12321161645, No. 12234007, No. 12221004, No. T2394480, and T2394481), the National Key R&D Program of China (2023YFA1406900 and 2022YFA1404800), the Science and Technology Commission of Shanghai Municipality (24142200100, 22142200400, 21DZ1101500, 2019SHZDZX01, and 23DZ2260100), and Hong Kong RGC (CRS_HKUST601/23 and AoE/P-502/20).

Notes

J.C.; W.L.; J.W.; R.-Y.Z.; X.C.; F.G.; L.S.; J.Z.; C.T.C. Topological Singularities in Metasurface Scattering Matrices: From Nodal Lines to Exceptional Lines. 2024. arXiv:2411.04666. arXiv. https://arxiv.org/abs/2411.04666 (accessed April 30, 2025).

The authors declare no competing financial interest.

■ ACKNOWLEDGMENTS

The authors would like to thank Profs. Meng Xiao and Dezhuan Han for helpful discussions. Claude-3.5-Sonnet is used for language and grammar cleanup.

■ REFERENCES

(1) Qi, X.-L.; Zhang, S.-C. Topological insulators and superconductors. *Rev. Mod. Phys.* **2011**, *83*, 1057−1110.

(2) Ochiai, T.; Onoda, M. Photonic analog of graphene model and its extension: Dirac cone, symmetry, and edge states. *Phys. Rev. B* **2009**, *80*, No. 155103.

(3) Lu, L.; Joannopoulos, J. D.; Soljačić, M. *Topological photonics. Nat. Photon.* **2014**, *8*, 821−829.

(4) Gao, W.; Lawrence, M.; Yang, B.; Liu, F.; Fang, F.; Béri, B.; Li, J.; Zhang, S. Topological Photonic Phase in Chiral Hyperbolic Metamaterials. *Phys. Rev. Lett.* **2015**, *114*, No. 037402.

(5) He, C.; Sun, X.-C.; Liu, X.-P.; Lu, M.-H.; Chen, Y.; Feng, L.; Chen, Y.-F. Photonic topological insulator with broken time-reversal symmetry. *Proc. Natl. Acad. Sci. U. S. A.* **2016**, *113*, 4924−4928.

(6) Parappurath, N.; Alpeggiani, F.; Kuipers, L.; Verhagen, E. Direct Observation of Topological Edge States in Silicon Photonic Crystals: Spin, dispersion, and chiral routing. *Sci. Adv.* **2020**, *6*, No. eaaw4137.

(7) Liu, G.-G.; Zhou, P.; Yang, Y.; Xue, H.; Ren, X.; Lin, X.; Sun, H.-X.; Bi, L.; Chong, Y.; Zhang, B. Observation of an unpaired photonic Dirac point. *Nat. Commun.* **2020**, *11*, 1873.

(8) Yang, E.; Yang, B.; You, O.; Chan, H.-C.; Mao, P.; Guo, Q.; Ma, S.; Xia, L.; Fan, D.; Xiang, Y.; Zhang, S. Observation of Non-Abelian Nodal Links in Photonics. *Phys. Rev. Lett.* **2020**, *125*, No. 033901.

(9) Guo, Q.; Jiang, T.; Zhang, R.-Y.; Zhang, L.; Zhang, Z.-Q.; Yang, B.; Zhang, S.; Chan, C. T. Experimental observation of non-Abelian topological charges and edge states. *Nature* **2021**, *594*, 195−200.

(10) Ota, Y.; Katsumi, R.; Watanabe, K.; Iwamoto, S.; Arakawa, Y. Topological photonic crystal nanocavity laser. *Commun. Phys.* **2018**, *1*, 86.

(11) Gao, X.; Yang, L.; Lin, H.; Zhang, L.; Li, J.; Bo, F.; Wang, Z.; Lu, L. Dirac-vortex topological cavities. *Nat. Nanotechnol.* **2020**, *15*, 1012−1018.

(12) Shao, Z.-K.; Chen, H.-Z.; Wang, S.; Mao, X.-R.; Yang, Z.-Q.; Wang, S.-L.; Wang, X.-X.; Hu, X.; Ma, R.-M. A high-performance topological bulk laser based on band-inversion-induced reflection. *Nat. Nanotechnol.* **2020**, *15*, 67−72.

(13) Yang, L.; Li, G.; Gao, X.; Lu, L. Topological-cavity surface-emitting laser. *Nat. Photonics* **2022**, *16*, 279−283.

(14) Feshbach, H. Unified Theory of Nuclear Reactions. *Rev. Mod. Phys.* **1964**, *36*, 1076−1078.

(15) Fano, U. Effects of Configuration Interaction on Intensities and Phase Shifts. *Phys. Rev.* **1961**, *124*, 1866−1878.

(16) Miroshnichenko, A. E.; Flach, S.; Kivshar, Y. S. Fano resonances in nanoscale structures. *Rev. Mod. Phys.* **2010**, *82*, 2257−2298.

(17) Yao, S.; Song, F.; Wang, Z. Non-Hermitian Chern Bands. *Phys. Rev. Lett.* **2018**, *121*, No. 136802.

(18) Shen, H.; Zhen, B.; Fu, L. Topological Band Theory for Non-Hermitian Hamiltonians. *Phys. Rev. Lett.* **2018**, *120*, No. 146402.

(19) Okuma, N.; Kawabata, K.; Shiozaki, K.; Sato, M. Topological Origin of Non-Hermitian Skin Effects. *Phys. Rev. Lett.* **2020**, *124*, No. 086801.

(20) Zhou, Q.; Wu, J.; Pu, Z.; Lu, J.; Huang, X.; Deng, W.; Ke, M.; Liu, Z. Observation of geometry-dependent skin effect in non-Hermitian phononic crystals with exceptional points. *Nat. Commun.* **2023**, *14*, 4569.

(21) Zhang, H.; Chen, T.; Li, L.; Lee, C. H.; Zhang, X. Electrical circuit realization of topological switching for the non-Hermitian skin effect. *Phys. Rev. B* **2023**, *107*, No. 085426.

(22) Wiersig, J. Enhancing the Sensitivity of Frequency and Energy Splitting Detection by Using Exceptional Points: Application to Microcavity Sensors for Single-Particle Detection. *Phys. Rev. Lett.* **2014**, *112*, No. 203901.

(23) Chen, W.; Özdemir, S. K.; Zhao, G.; Wiersig, J.; Yang, L. Exceptional points enhance sensing in an optical microcavity. *Nature* **2017**, *548*, 192−196.

(24) Hodaei, H.; Hassan, A. U.; Wittek, S.; Garcia-Gracia, H.; El-Ganainy, R.; Christodoulides, D. N.; Khajavikhan, M. Enhanced sensitivity at higher-order exceptional points. *Nature* **2017**, *548*, 187−191.

(25) Hokmabadi, M.; Schumer, A.; Christodoulides, D.; Khajavikhan, M. Non-Hermitian ring laser gyroscopes with enhanced Sagnac sensitivity. *Nature* **2019**, *576*, 70−74.

(26) Li, A.; Wei, H.; Cotrufo, M.; Chen, W.; Mann, S.; Ni, X.; Xu, B.; Chen, J.; Wang, J.; Fan, S.; Qiu, C.-W.; Alù, A.; Chen, L. Exceptional points and non-Hermitian photonics at the nanoscale. *Nat. Nanotechnol.* **2023**, *18*, 706−720.

(27) Lawrence, M.; Xu, N.; Zhang, X.; Cong, L.; Han, J.; Zhang, W.; Zhang, S. Manifestation of P T symmetry breaking in polarization

space with terahertz metasurfaces. *Phys. Rev. Lett.* **2014**, *113*, No. 093901.
(28) Song, Q.; Odeh, M.; Zúñiga Pérez, J.; Kanté, B.; Genevet, P. Plasmonic topological metasurface by encircling an exceptional point. *Science* **2021**, *373*, 1133−1137.
(29) Ding, K.; Fang, C.; Ma, G. Non-Hermitian topology and exceptional-point geometries. *Nat. Rev. Phys.* **2022**, *4*, 745−760.
(30) He, T.; Zhang, Z.; Zhu, J.; Shi, Y.; Li, Z.; Wei, H.; Wei, Z.; Li, Y.; Wang, Z.; Qiu, C.-W.; Cheng, X. Scattering exceptional point in the visible. *Light Sci. Appl.* **2023**, *12*, 229.
(31) Baek, S.; et al. Non-Hermitian chiral degeneracy of gated graphene metasurfaces. *Light Sci. Appl.* **2023**, *12*, 87.
(32) Yang, Z.; Huang, P.-S.; Lin, Y.-T.; Qin, H.; Zúñiga Pérez, J.; Shi, Y.; Wang, Z.; Cheng, X.; Tang, M.-C.; Han, S.; Kanté, B.; Li, B.; Wu, P. C.; Genevet, P.; Song, Q. Creating pairs of exceptional points for arbitrary polarization control: asymmetric vectorial wavefront modulation. *Nat. Commun.* **2024**, *15*, 232.
(33) Erb, J.; Shaibe, N.; Calvo, R.; Lathrop, D.; Antonsen, T.; Kottos, T.; Anlage, S. M. Novel Topology and Manipulation of Scattering Singularities in Complex non-Hermitian Systems. *arXiv* **2024**.
(34) Kravets, V. G.; Schedin, F.; Jalil, R.; Britnell, L.; Gorbachev, R. V.; Ansell, D.; Thackray, B.; Novoselov, K. S.; Geim, A. K.; Kabashin, A. V.; Grigorenko, A. N. Singular phase nano-optics in plasmonic metamaterials for label-free single-molecule detection. *Nat. Mater.* **2013**, *12*, 304−309.
(35) Malassis, L.; Massé, P.; Tréguer-Delapierre, M.; Mornet, S.; Weisbecker, P.; Barois, P.; Simovski, C. R.; Kravets, V. G.; Grigorenko, A. N. Topological Darkness in Self-Assembled Plasmonic Metamaterials. *Adv. Mater.* **2014**, *26*, 324−330.
(36) Guo, C.; Xiao, M.; Orenstein, M.; Fan, S. Structured 3D linear space−time light bullets by nonlocal nanophotonics. *Light Sci. Appl.* **2021**, *10*, 160.
(37) Ermolaev, G.; et al. Topological phase singularities in atomically thin high-refractive-index materials. *Nat. Commun.* **2022**, *13*, 2049.
(38) Tselikov, G. I.; Danilov, A.; Shipunova, V. O.; Deyev, S. M.; Kabashin, A. V.; Grigorenko, A. N. Topological Darkness: How to Design a Metamaterial for Optical Biosensing with Ultrahigh Sensitivity. *ACS Nano* **2023**, *17*, 19338−19348.
(39) Burkov, A. A.; Hook, M. D.; Balents, L. Topological nodal semimetals. *Phys. Rev. B* **2011**, *84*, No. 235126.
(40) Lim, L.-K.; Moessner, R. Pseudospin Vortex Ring with a Nodal Line in Three Dimensions. *Phys. Rev. Lett.* **2017**, *118*, No. 016401.
(41) Lin, J. Y.; Hu, N. C.; Chen, Y. J.; Lee, C. H.; Zhang, X. Line nodes, Dirac points, and Lifshitz transition in two-dimensional nonsymmorphic photonic crystals. *Phys. Rev. B* **2017**, *96*, No. 075438.
(42) Tiwari, A.; Bzdušek, T. Non-Abelian topology of nodal-line rings in PT-symmetric systems. *Phys. Rev. B* **2020**, *101*, No. 195130.
(43) Guo, C.; Li, J.; Xiao, M.; Fan, S. Singular topology of scattering matrices. *Phys. Rev. B* **2023**, *108*, No. 155418.
(44) Heiss, W. D. The physics of exceptional points. *J. Phys. A: Math. Theor.* **2012**, *45*, 444016.
(45) Longhi, S. PT-symmetric laser absorber. *Phys. Rev. A* **2010**, *82*, No. 031801.
(46) Chong, Y. D.; Ge, L.; Stone, A. D. PT-Symmetry Breaking and Laser-Absorber Modes in Optical Scattering Systems. *Phys. Rev. Lett.* **2011**, *106*, No. 093902.
(47) Kirillov, O. N.; Mailybaev, A. A.; Seyranian, A. P. Unfolding of eigenvalue surfaces near a diabolic point due to a complex perturbation. *J. Phys. A: Math. Gen.* **2005**, *38*, 5531−5546.
(48) Kozii, V.; Fu, L. Non-Hermitian Topological Theory of Finite-Lifetime Quasiparticles: Prediction of Bulk Fermi Arc Due to Exceptional Point. *arXiv* **2017**.
(49) Zhou, H.; Peng, C.; Yoon, Y.; Hsu, C. W.; Nelson, K. A.; Fu, L.; Joannopoulos, J. D.; Soljačić, M.; Zhen, B. Observation of bulk Fermi arc and polarization half charge from paired exceptional points. *Science* **2018**, *359*, 1009−1012.
(50) Xu, Y.; Li, L.; Jeong, H.; Kim, S.; Kim, I.; Rho, J.; Liu, Y. Subwavelength control of light transport at the exceptional point by non-Hermitian metagratings. *Sci. Adv.* **2023**, *9*, No. eadf3510.
(51) Qin, H.; et al. Sphere of arbitrarily polarized exceptional points with a single planar metasurface. *Nat. Commun.* **2025**, *16*, 2656.

https://doi.org/10.1021/acsphotonics.5c00575
ACS Photonics XXXX, XXX, XXX−XXX